High Activities of Hydrogen Peroxide Decomposition Catalyzed by Dinuclear Schiff Base Mn(III)–Cu(II) Complexes Accompanying Metal Substitution in *N,N*-Dimethylformamide and the Crystal Structure of a Substituted Schiff Base Cu(II) Complex

Minori Uehara, Mika Urade, Atsuko Ueda, Narumi Sakagami†, and Yuriko Abe*

Department of Chemistry, Faculty of Science, Nara Women's University, Nara 630

†Department of Chemistry, University of Tsukuba, Tsukuba 305

(Received December 19, 1997)

The effects of divalent metal ions (M^{2+} = Mn^{2+}, Co^{2+}, Ni^{2+}, Cu^{2+}, and Zn^{2+} ions) on the catalase-like activities of mononuclear Schiff base Mn(III) complexes, such as [Mn(salen)Cl] (H_2salen: *N,N'*-ethylenebis(salicylideneamine)), [Mn(saltn)Cl] (H_2saltn: *N,N'*-propane-1,3-diylbis(salicylideneamine)), [Mn(saltnOH)Cl] (H_2saltnOH: *N,N'*-(2-hydroxypropane-1,3-diyl)bis(salicylideneamine)), and [Mn(saltnOCOPh)Cl] (H_2saltnOCOPh: *N,N'*-(2-benzoyloxypropane-1,3-diyl)bis(salicylideneamine)), in *N,N*-dimethylformamide (DMF) have been reported. Except for the Cu^{2+} ion, H_2O_2 decomposition was depressed in the presence of M^{2+} = Mn^{2+}, Co^{2+}, Ni^{2+}, and Zn^{2+} ions because $[Mn(salen)]^+$ reacted with M^{2+} to give dinuclear Mn(III)–M(II) and trinuclear $Mn(III)_2$–M(II) complexes inactive toward H_2O_2 in DMF. For the Cu^{2+} ion, the dinuclear complexes with the salen and saltnOCOPh ligands showed high activities, although the trinuclear complexes were inactive toward H_2O_2. The ESR spectra suggested that the intramolecular electron transfer from Cu(II) to Mn(III) on the dinuclear Mn(III)–Cu(II) complex partly occurs to produce a dinuclear Mn(II)–Cu(III) complex active toward H_2O_2. During H_2O_2 decomposition including the radical reaction path, [Cu(salR)] (R = en, tnOCOPh) and Mn^{2+} were produced accompanying metal substitution by Cu^{2+} on the dinuclear complex. To clarify the substituted product, the preparation and an X-ray crystal structure analysis of [Cu(saltnOCOPh)] were carried out. Three independent [Cu(saltnOCOPh)] complexes (CuA, CuB, and CuC) were present along with an intermolecular π–π stacking interaction between benzene rings on the salicylidenediamine moiety and benzene ring on the benzoyloxy group in the crystal. The geometries around the coppers in both CuA and CuC are more distorted toward tetrahedral from square plane than that in CuB. No stacking interaction between benzene rings on [Cu(saltnOCOPh)] occurs in DMF solution.

In a previous paper[1] we reported on the kinetics and mechanisms of manganese catalase (Mn–CAT)-like activities of mononuclear Schiff base Mn(III) complexes, such as [Mn(salen)Cl] (H_2salen: *N,N'*-ethylenebis(salicylideneamine)), [Mn(saltn)Cl] (H_2saltn: *N,N'*-propane-1,3-diylbis(salicylideneamine)), [Mn(saltnOH)Cl] (H_2saltnOH: *N,N'*-(2-hydroxypropane-1,3-diyl)bis(salicylideneamine)), and [Mn(saltnOCOPh)Cl] (H_2saltnOCOPh: *N,N'*-(2-benzoyloxypropane-1,3-diyl)bis(salicylideneamine)), coupled by the Mn(III)–Mn(IV) redox cycle in *N,N*-dimethylformamide (DMF). Mn–CAT catalyzes the disproportionation of H_2O_2 to O_2 and H_2O in biological systems.[2] The addition of the OH^- ion to a $[Mn(salen)]^+$ solution caused the reaction path by the Mn(II)–Mn(III) redox couple, similar to biological systems due to the formation of the [Mn(salen)OH] complex.[3] This result was accounted by a significant change in the redox potential of the Mn complex. It is of great interest to investigate the effects of transition-metal ions on the catalase-like activities of Schiff base Mn(III) complexes in DMF. Because two phenoxo oxygens on the Schiff base complex have a coordination ability, the Schiff base complex behaves as a didentate ligand. [M(salen)] (M = Cu(II), Ni(II), or Zn(II)) reacts with $M'X_2$ and $M'(ClO_4)_2$ (M' = Mn(II), Fe(II), Co(II), Ni(II), Cu(II), or Zn(II)) to give polynuclear Schiff base complexes, such as $[M(salen)M'Cl_2]$ and $[M(salen)M'(salen)M](ClO_4)_2$,[4,5] respectively. Thus, the reaction of Schiff base Mn(III) complexes with M^{2+} may also afford the dinuclear Mn(III)–M(II) (Scheme 1) and trinuclear $Mn(III)_2$–M(II)-Schiff base complexes in DMF. It is suggested that the catalase-like activities of the polynuclear complexes may be significantly different from those of the mononuclear complexes on account of the change in the electron density of the Mn^{3+} ion, which is produced from the coordination of the M^{2+} ion to two phenoxo oxygens on the polynuclear complexes. Polynuclear metal complexes have attracted great interest in elucidating the magnetic coupling between metals[6] and in functional model compounds of the active site in metalloenzymes.[7,8] From these viewpoints, we have examined the effects of M^{2+} = Mn^{2+}, Co^{2+}, Ni^{2+}, Cu^{2+}, and Zn^{2+} on the catalase-like activities of $[Mn(salen)]^+$ in DMF. For the Cu^{2+} ion, since a large acceleration effect was observed to accompany a metal-substitution reaction by the Cu^{2+} ion on the dinuclear complex, the catalytic effects of $[Mn(saltn)]^+$, $[Mn(saltnOH)]^+$, and $[Mn(saltnOCOPh)]^+$

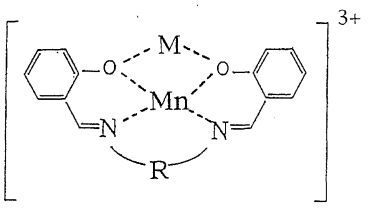

ligand	-R-
salen:	-CH_2CH_2-
saltn:	-$CH_2CH_2CH_2$-
saltnOH:	-$CH_2CH(OH)CH_2$-
saltnOCOPh:	-CH_2CHCH$_2$-

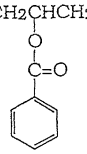

Scheme 1. Proposed structure of dinuclear $[Mn(salR)M]^{3+}$ (M = Mn, Co, Ni, Cu, and Zn) in DMF. Solvent is omitted.

with the six-membered ring on the 1,3-diamine moiety have been investigated. Further, the preparation and an X-ray crystal structure analysis of [Cu(saltnOCOPh)] was reported in order to clarify the substituted product.

Experimental

Materials and Procedures for Kinetic Studies. All Chemicals were of reagent grade. Schiff base complexes ([Mn(salen)Cl],[9] [Mn(saltnOCOPh)Cl]·DMF,[1] [Cu(salen)],[9] and [Cu(saltnOH)][10]) were prepared as described. [Mn(saltn)Cl] and [Mn(saltnOH)Cl] were prepared by modifying the method of Bonadies et al.[11] $[M(ClO_4)_2]\cdot 6DMF$ (M = Mn, Co, Ni, Cu, and Zn) was obtained by modifying the preparation method of Donoghue et al.[12] Hydrogen peroxide and potassium permanganate were used without further purification. Tetra-*n*-butylammonium perchlorate was recrystallized from ethanol. DMF was purified as described.[13] The reaction was followed by a decrease in the H_2O_2 concentration by titration with a $KMnO_4$ solution after passing aliquots of the reaction solution through a cation ion-exchange resin (Dowex 50×8, 50—100 mesh) at regular time intervals. The evolved dioxygen was collected with a gas burette. The ionic strength was adjusted to 0.01 mol dm^{-3} with tetra-*n*-butylammonium perchlorate.

Physical Measurements. Infrared and UV spectra were recorded on a JASCO FT/IR-8900μ spectrophotometer using KBr disks and a Shimadzu UV-3100 spectrophotometer, respectively. Cyclic voltammograms were recorded by using a Hokuto Denko HZ-1A apparatus. Measurements were carried out in DMF solution containing tetra-*n*-butylammonium perchlorate (0.1 mol dm^{-3}) as the supporting electrolyte. A three-electrode cell was used which was equipped with a glassy carbon working electrode, a platinum as the counter electrode, and an $Ag/AgPF_6$ electrode as the reference. ESR spectra were recorded on a JEOL RE-3X ESR spectrometer on frozen DMF solution at liquid nitrogen temperature.

Preparation of [Cu(saltnOCOPh)]. [Cu(saltnOCOPh)] was prepared as follows: [Cu(saltnOH)][10] (2 mmol) was reacted with benzoic anhydride (4 mmol) in the presence of 4-*N*,*N*-dimetyl aminopyridine (2 mmol) in a mixture (50 cm^3) of a CH_3CN(AN)–DMF (1 : 1 v/v). After stirring at room temperature for 2 d, the solution was evaporated and a crude crystalline product was collected by filtration, which was purified through a column of silica gel by using the eluent of a dichloromethane–methanol (4 : 1 v/v). A single crystal suitable for the X-ray measurement was obtained by slow evaporation of AN solution at room temperature. Calcd for $CuC_{24}N_2O_4H_{21}$: C; 62.14, N; 4.31, H; 6.04%. Found: C; 61.75, N; 4.46, H; 6.05%.

Crystal Structure Analysis for [Cu(saltnOCOPh)]. All measurements were made on an Enraf–Nonius CAD4 diffractometer with graphite monochomated Mo $K\alpha$ raditation at room temperature. Data were corrected for Lorentz and polarization effects. The structure was solved by a direct method,[14] expanded using Fourier techniques[15] and refined by a full-matrix least-squares analysis using the teXsan crystallographic software package. The non-hydrogen atoms were refined anisotropically. Hydrogen atoms were included, but not refined. The crystal data, intensity collection and structural refinement are summarized in Table 1, and the atomic parameters of the non-hydrogen atoms are given in Table 2.

Results and Discussion

Crystal Structure of [Cu(saltnOCOPh)]. As mentioned in the section below, for the Cu^{2+} ion, a large acceleration effect for H_2O_2 decomposition reaction was observed to accompany a metal-substitution reaction by the Cu^{2+} ion on the dinuclear complex. In order to clarify the substituted product, the preparation and an X-ray crystal structure analysis of [Cu(saltnOCOPh)] were performed. The IR spectrum of [Cu(saltnOCOPh)] on KBr disks exhibited a new intense band at 1722 cm^{-1} due to the replacement of a hydroxy group by a benzoyloxy group on the 1,3-diamine ring. An

Table 1. Crystallographic and Experimental Data for [Cu(saltnOCOPh)]

Formula	$CuC_{24}N_2O_4H_{21}$
Formula weight	464.99
Cryst. color, habit	Brown, needle
Cryst. size/mm	0.35 × 0.18 × 0.15
Cryst. system	Monoclinic
Space group	$P2_1/n$ (No. 14)
a/Å	21.48(1)
b/Å	11.763(2)
c/Å	26.62(1)
β/deg	113.7(2)
V/Å^3	6161(3)
Z	12
T/°C	23 ± 1
D_{calcd}/g cm^{-3}	1.504
F_{000}	4036
μ(Mo $K\alpha$)/cm^{-1}	11.0
Machine	Enraf–Nonius CAD4
Radiation	Mo $K\alpha$
Take-off angle/deg	2.8
Scan type	ω–2θ
$2\theta_{max}$/deg	50.0
No. of measured reflections	11666
No. of unique reflections	11479
No. of variables	839
Trans. factors range	0.96—1.00
Refinement	Full-matrix least-squares
R[a]	0.041
R_w[b]	0.054

a) $R = (\Sigma||F_o| - |F_c||)/\Sigma|F_o|$.
b) $R_w = (\Sigma w(|F_o| - |F_c|)^2/\Sigma w|F_o|^2)^{1/2}$.

Table 2. Positional Parameters and B(eq) for [Cu(saltnOCOPh)]

Atom	x	y	z	B(eq)	Atom	x	y	z	B(eq)
Cu(A)	0.67105(5)	−0.14109(9)	0.33982(4)	3.01(2)	C(10c)	0.7469(5)	0.1505(8)	0.4425(3)	4.4(3)
Cu(B)	0.48871(5)	0.36125(9)	0.48815(4)	2.84(2)	C(11a)	0.8819(4)	−0.1022(7)	0.4095(3)	3.8(2)
Cu(C)	0.66247(5)	0.13852(9)	0.32731(4)	3.25(3)	C(11b)	0.5881(4)	0.4388(8)	0.6542(3)	3.8(2)
O(1a)	0.6540(3)	−0.0996(5)	0.2664(2)	3.3(1)	C(11c)	0.7520(5)	0.1598(8)	0.4969(4)	5.4(3)
O(1b)	0.3975(2)	0.3742(5)	0.4838(2)	3.2(1)	C(12a)	0.9367(4)	−0.1050(8)	0.4579(4)	4.5(3)
O(1c)	0.5745(3)	0.0855(5)	0.3172(2)	3.7(1)	C(12b)	0.6513(5)	0.4262(9)	0.6966(3)	4.9(3)
O(2a)	0.7649(2)	−0.1155(5)	0.3572(2)	3.6(1)	C(12c)	0.8136(6)	0.1821(10)	0.5388(4)	6.3(3)
O(2b)	0.5185(3)	0.4259(5)	0.5605(2)	3.7(1)	C(13a)	0.9282(4)	−0.1222(8)	0.5067(3)	4.9(2)
O(2c)	0.6875(3)	0.1267(5)	0.4040(2)	4.2(2)	C(13b)	0.7081(4)	0.3908(9)	0.6887(3)	5.0(3)
O(3a)	0.5031(2)	−0.1664(5)	0.3849(2)	3.8(1)	C(13c)	0.8720(6)	0.197(1)	0.5299(4)	6.8(3)
O(3b)	0.5234(3)	0.3342(5)	0.3458(2)	4.1(2)	C(14a)	0.8645(4)	−0.1352(8)	0.5041(3)	4.3(2)
O(3c)	0.7031(2)	0.1506(5)	0.1875(2)	3.9(1)	C(14b)	0.7000(4)	0.3707(8)	0.6367(3)	4.1(2)
O(4a)	0.5101(3)	−0.1375(6)	0.4706(2)	5.2(2)	C(14c)	0.8680(5)	0.1911(8)	0.4787(4)	5.2(3)
O(4b)	0.6232(3)	0.3805(5)	0.3420(2)	4.7(2)	C(15a)	0.5764(4)	−0.2851(7)	0.3629(3)	3.8(2)
O(4c)	0.8036(3)	0.1235(6)	0.1819(2)	5.1(2)	C(15b)	0.5119(4)	0.2081(8)	0.4107(3)	3.8(2)
N(1a)	0.5842(3)	−0.2193(5)	0.3185(2)	2.8(2)	C(15c)	0.6810(4)	0.2772(7)	0.2448(3)	3.8(2)
N(1b)	0.4586(3)	0.2699(6)	0.4211(3)	3.3(2)	C(16a)	0.5720(4)	−0.2148(8)	0.4090(3)	3.5(2)
N(1c)	0.6309(3)	0.2070(6)	0.2552(2)	3.0(2)	C(16b)	0.5614(4)	0.2842(8)	0.3997(3)	3.2(2)
N(2a)	0.6836(3)	−0.1348(6)	0.4160(2)	3.3(2)	C(16c)	0.7375(4)	0.2081(8)	0.2395(3)	3.6(2)
N(2b)	0.5818(3)	0.3665(5)	0.4931(2)	3.0(2)	C(17a)	0.6224(4)	−0.1179(7)	0.4276(3)	3.8(2)
N(2c)	0.7570(3)	0.1436(6)	0.3349(3)	3.1(2)	C(17b)	0.5920(4)	0.3789(8)	0.4411(3)	3.8(2)
C(1a)	0.5387(4)	−0.2263(7)	0.2690(3)	3.3(2)	C(17c)	0.7691(4)	0.1216(8)	0.2843(3)	4.0(2)
C(1b)	0.3965(4)	0.2597(7)	0.3864(3)	3.6(2)	C(18a)	0.4771(4)	−0.1336(8)	0.4216(3)	3.7(2)
C(1c)	0.5717(5)	0.1905(8)	0.2164(3)	3.7(2)	C(18b)	0.5620(5)	0.3767(8)	0.3210(3)	4.0(2)
C(2a)	0.5422(4)	−0.1792(7)	0.2208(3)	3.1(2)	C(18c)	0.7425(5)	0.1179(7)	0.1615(3)	3.7(2)
C(2b)	0.3375(4)	0.3004(7)	0.3932(3)	3.6(2)	C(19a)	0.4061(4)	−0.0915(7)	0.3942(3)	3.4(2)
C(2c)	0.5164(4)	0.1313(8)	0.2209(3)	3.6(2)	C(19b)	0.5201(5)	0.4180(8)	0.2648(3)	3.8(2)
C(3a)	0.6009(4)	−0.1244(8)	0.2231(3)	3.4(2)	C(19c)	0.7009(4)	0.0754(8)	0.1052(3)	3.5(2)
C(3b)	0.3416(4)	0.3471(7)	0.4426(3)	3.2(2)	C(20a)	0.3659(4)	−0.1148(8)	0.3397(4)	4.5(2)
C(3c)	0.5201(4)	0.0853(8)	0.2711(4)	3.4(2)	C(20b)	0.4513(5)	0.3902(9)	0.2383(3)	5.0(3)
C(4a)	0.6015(4)	−0.0957(7)	0.1717(3)	4.1(2)	C(20c)	0.6334(4)	0.1016(8)	0.0784(4)	4.1(2)
C(4b)	0.2793(4)	0.3678(8)	0.4476(4)	4.7(2)	C(21a)	0.2997(5)	−0.0747(9)	0.3168(4)	5.2(3)
C(4c)	0.4603(5)	0.0370(9)	0.2712(4)	5.0(3)	C(21b)	0.4169(5)	0.424(1)	0.1841(4)	6.3(3)
C(5a)	0.5464(5)	−0.1173(9)	0.1234(3)	5.6(3)	C(21c)	0.5980(5)	0.0653(9)	0.0251(4)	5.1(3)
C(5b)	0.2188(5)	0.3454(9)	0.4059(5)	6.1(3)	C(22a)	0.2737(5)	−0.0163(9)	0.3490(5)	5.5(3)
C(5c)	0.4020(5)	0.0317(9)	0.2248(5)	5.7(3)	C(22b)	0.4491(7)	0.484(1)	0.1583(4)	6.3(3)
C(6a)	0.4881(5)	−0.1685(9)	0.1235(4)	5.3(3)	C(22c)	0.6294(6)	−0.0013(9)	0.0000(4)	5.2(3)
C(6b)	0.2155(5)	0.305(1)	0.3563(5)	6.8(3)	C(23a)	0.3130(5)	0.0043(10)	0.4026(4)	5.9(3)
C(6c)	0.3990(5)	0.0739(10)	0.1758(4)	5.9(3)	C(23b)	0.5158(6)	0.5156(9)	0.1846(4)	5.5(3)
C(7a)	0.4871(4)	−0.1989(8)	0.1715(4)	4.2(2)	C(23c)	0.6965(6)	−0.0279(9)	0.0266(4)	5.6(3)
C(7b)	0.2738(5)	0.2811(9)	0.3496(4)	5.5(3)	C(24a)	0.3791(5)	−0.0340(9)	0.4258(4)	5.0(3)
C(7c)	0.4552(5)	0.1228(9)	0.1736(4)	5.2(3)	C(24b)	0.5513(5)	0.4826(8)	0.2376(4)	4.5(3)
C(8a)	0.7413(4)	−0.1337(8)	0.4576(3)	3.4(2)	C(24c)	0.7329(4)	0.0098(8)	0.0791(4)	4.6(3)
C(8b)	0.6358(4)	0.3684(7)	0.5377(3)	3.2(2)	H(1A)	0.5632	−0.1541	0.3260	3.3650
C(8c)	0.8082(4)	0.1601(8)	0.3808(3)	3.9(2)	H(1B)	0.4643	0.3336	0.4013	3.9185
C(9a)	0.8064(4)	−0.1323(8)	0.4549(3)	3.3(2)	H(1C)	0.6487	0.1423	0.2425	3.8874
C(9b)	0.6380(4)	0.3808(7)	0.5915(3)	2.8(2)	H(2A)	0.6802	−0.2152	0.4178	3.9755
C(9c)	0.8060(4)	0.1704(7)	0.4335(3)	3.5(2)	H(2B)	0.5835	0.2859	0.4912	3.6404
C(10a)	0.8149(4)	−0.1169(7)	0.4054(3)	3.2(2)	H(2C)	0.7534	0.2230	0.3276	3.7436
C(10b)	0.5799(4)	0.4130(7)	0.6006(3)	3.0(2)	H(3A)	0.4985	−0.2672	0.2641	3.9935

X-ray study showed that this crystal contains three independent [Cu(saltnOCOPh)] molecules (CuA, CuB, and CuC). An ORTEP drawing of CuA is illustrated in Fig. 1A. Selected intramolecular bond distances and angles of CuA, CuB, and CuC are listed in Table 3. Among the three molecules, the bond distances and angles in CuA resemble the corresponding bond distances and angles in CuC, as shown in Table 3. However, the bond distances of Cu–O1 [1.923(5) Å], Cu–O2 [1.926(5) Å], and Cu–N1 [1.958(6) Å] and the angles of O1–Cu–N2 [173.6(2)°] and O2–Cu–N1[169.8(3)°] in CuB are much larger than those in CuA and CuC. The geometries around the copper are described as a square plane significantly distorted toward tetrahedral with N_2O_2 donor atoms of a tetradentate Schiff base ligand. Although such a trend has also been found for the [Cu(saltnOH)],[10] the distortion in the [Cu(saltnOCOPh)] is much milder, especially for the CuB complex. That is, the dihedral angles between the O1–Cu–N1 and O2–Cu–N2 planes are 27.31°, 18.31°, and 27.63° for

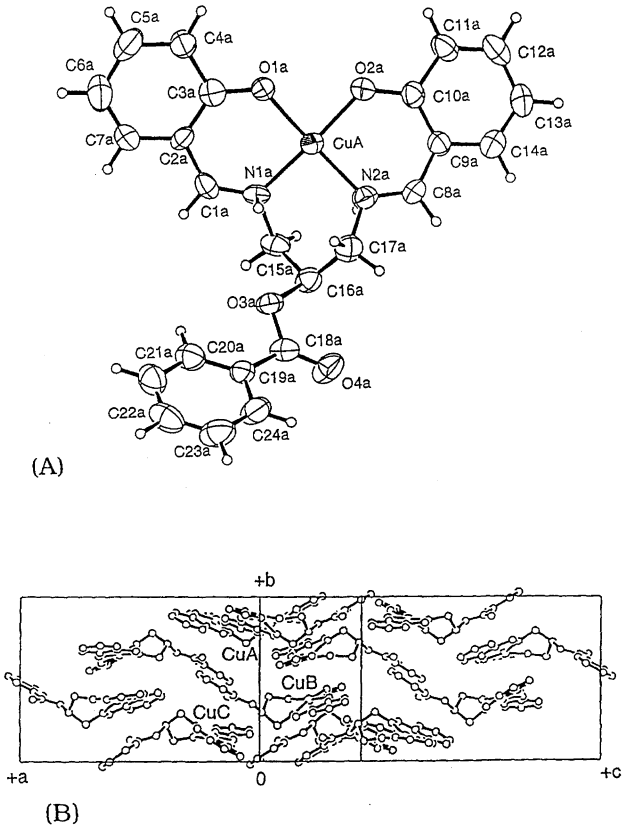

Fig. 1. (A) ORTEP drawing of CuA for [Cu(saltnOCOPh)] and (B) Molecular packing diagram of [Cu(saltnOCOPh)] as viewed along the *b*-axis.

Table 3. Selected Intramolecular Bond Distances (Å) and Angles (°)

	CuA	CuB	CuC
Cu–O1	1.902(5)	1.923(5)	1.903(4)
Cu–O2	1.902(5)	1.926(5)	1.897(5)
Cu–N1	1.949(6)	1.958(6)	1.937(6)
Cu–N2	1.937(6)	1.951(6)	1.959(6)
N1–C15	1.479(8)	1.47(1)	1.469(9)
N2–C17	1.480(9)	1.492(9)	1.492(9)
C15–C16	1.51(1)	1.51(1)	1.51(1)
C16–C17	1.51(1)	1.52(1)	1.51(1)
O1–Cu–O2	87.5(2)	87.1(3)	88.0(2)
O1–Cu–N1	93.2(2)	91.9(2)	93.6(3)
O1–Cu–N2	162.7(3)	173.6(2)	162.4(3)
O2–Cu–N1	160.5(2)	169.8(3)	158.9(3)
O2–Cu–N2	92.9(2)	90.0(2)	93.3(2)
N1–Cu–N2	92.1(3)	91.9(3)	91.5(3)
Cu–N1–C15	114.7(5)	116.4(5)	115.4(5)
Cu–N2–C17	117.5(5)	117.9(5)	116.8(5)
N1–C15–C16	115.2(7)	113.9(7)	113.0(7)
N2–C17–C16	114.2(7)	114.2(7)	114.9(7)
C15–C16–C17	114.4(7)	115.3(6)	114.4(7)

the CuA, CuB and CuC, and 35.7° for the [Cu(saltnOH)], respectively. O1–Cu–O2 is much smaller and O1–Cu–N2 and O2–Cu–N1 are much larger than those of the [Cu(saltnOH)] complex, reflecting the milder distortion.[10] Figure 1B shows a packing diagram of the unit cell as viewed along the *b*-axis. There are twelve molecules in a unit cell, which consist of two sets of structures with mirror images with respect to CuA, CuB, and CuC. The selected intermolecular distances between benzene rings on the salicylidenediamine moiety and on the benzoyloxy group are in the range of 3.46 to 3.59 Å as shown in Table 4. An intermolecular π–π stacking interaction exists in the crystal. That is, one of the benzene rings on the salicylidenediamine moiety of a CuB is stacked with a benzene ring on the benzoyloxy group in the neighboring CuA, and at the same time a benzene ring on the benzoyloxy group in the CuB is stacked with one of the benzene rings on the salicylidenediamine moiety of the neighboring CuC. These interactions result in larger bond distances and angles, and a smaller dihedral angle for the CuB compared with CuA and CuC. Most of the [Cu(salen)]-type complexes are square-planer[16] with a few examples of the tetradentate Schiff base copper(II) complex with large dihedral angles.[17,18] In these complexes, no stacking interaction was observed because of their large distortion, while square-planer [Cu(salen)] is likely to form stacking in the crystals. By introducing the benzene group to the 1,3-diamine ring, it may be possible to form a new intermolecular π–π stacking interaction.

[Cu(saltnOCOPh)] in DMF solution exhibits an electronic spectrum with two absorption bands at 372 nm ($\varepsilon = 11800$ $mol^{-1}\,dm^3\,cm^{-1}$) and 611 nm ($\varepsilon = 273$ $mol^{-1}\,dm^3\,cm^{-1}$), whereas [Cu(saltnOH)] as a starting material has similar bands at 370 nm ($\varepsilon = 11300$ $mol^{-1}\,dm^3\,cm^{-1}$), and 611 nm ($\varepsilon = 263$ $mol^{-1}\,dm^3\,cm^{-1}$).[10] These results suggest that the structure of [Cu(saltnOCOPh)] in DMF solution very closely resembles that of [Cu(saltnOH)] with the dihedral angle at 35.7°.[10] Thus, no stacking interactions between benzene rings on [Cu(saltnOCOPh)] may occur in DMF solution.

Effective Inhibition of Mn^{2+}, Co^{2+}, Ni^{2+}, and Zn^{2+} on Catalase-Like Activities of [Mn(salen)]$^+$ in DMF. Figure 2A shows the time courses of the decrease in the H_2O_2 concentration catalyzed by $[[Mn(salen)]^+]_0 = 2.00\times10^{-4}$ mol dm^{-3}in the absence and presence of Mn^{2+} in DMF. The decreases in the H_2O_2 concentration with time are depressed with increasing the Mn^{2+} concentration. Plots of the initial rate (v_0) vs. the M^{2+} concentration for Mn^{2+}, Co^{2+}, Ni^{2+}, and Zn^{2+} (Fig. 2B) indicate that the catalytic reactions are effectively inhibited by Co^{2+}, Ni^{2+}, and Zn^{2+} above $[M^{2+}]_0 = 1\times10^{-4}$ mol dm^{-3}. As can be seen in Fig. 3, cyclic voltammograms for [Mn(salen)]$^+$ show the shifts of the potentials of Mn(II)–Mn(III) and Mn(III)–Mn(IV) redox couples to higher values with increasing the Mn^{2+} concentration,

Table 4. Selected Intermolecular Distances (Å)

C19a···C9b	3.59(1)
C20a···C13b	3.56(1)
C20a···C14b	3.49(1)
C23a···C7b	3.51(2)
C20b···C2c	3.46(1)
C19b···C2c	3.56(1)

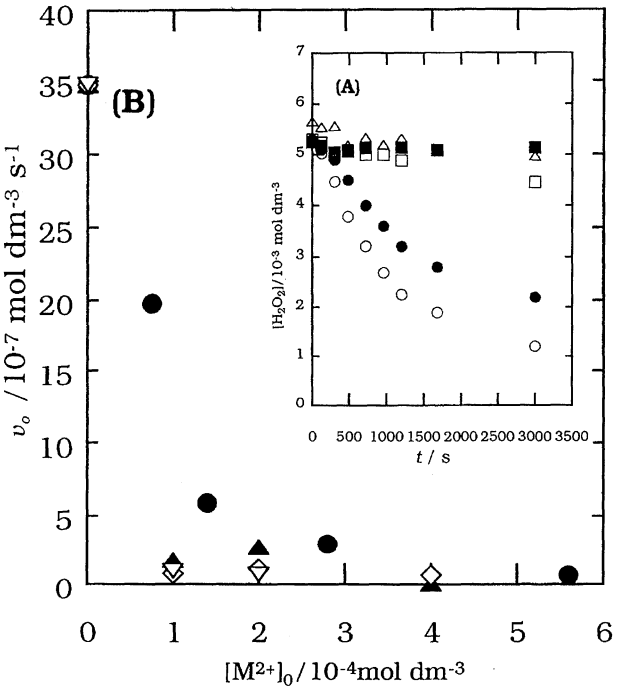

Fig. 2. (A) Time courses of H_2O_2 decomposition catalyzed by $[Mn(salen)]^+$ in the absence and presence of Mn^{2+} in DMF. $[H_2O_2]_0 = (5—5.5)$ mmol dm^{-3}, $[[Mn(salen)]^+]_0 =$ 0.200 mmol dm^{-3}, $[Mn^{2+}]_0$ = /mmol dm^{-3}: (○); 0, (●); 0.06, (□); 0.14, (△); 0.28, (■); 0.56. (B) Plots of v_0 vs. $[M^{2+}]_0$. (●); Mn^{2+}, (▲); Co^{2+}, (◇); Ni^{2+}, (▽); Zn^{2+}.

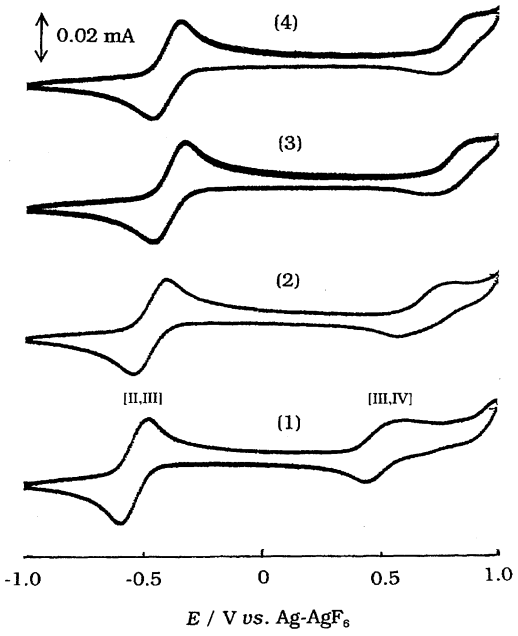

Fig. 3. Dependence of the Mn^{2+} concentration on the cyclic voltammogram. $[[Mn(salen)]^+]_0 = 3.00$ mmol dm^{-3}, $[Mn^{2+}]_0$ /mmol dm^{-3}: (1); 0, (2); 3.00, (3); 6.00, (4); 9.00.

with essentially similar data obtained for Co^{2+}, Ni^{2+}, and Zn^{2+} ions. In the absence of H_2O_2, the metal substitution by Mn^{2+}, Co^{2+}, Ni^{2+}, and Zn^{2+} on $[Mn(salen)]^+$ did not occur in DMF, because the addition of M^{2+} to the $[Mn(salen)]^+$ solution caused little spectral change in DMF. Accordingly, these changes in the cyclic voltammograms are due to the formation of the di- (Scheme 1) and trinuclear complexes. For the Mn^{2+} ion, the H_2O_2 decomposition is nearly inhibited by 2-fold concentrations of the Mn^{2+} ion over $[Mn(salen)]^+$ of which the potentials of Mn(II)–Mn(III) and Mn(III)–Mn(IV) redox cycles are little shifted, where the dinuclear complex is almost formed in DMF. Positive shifts result from a decrease in the electronic density of Mn^{3+} on the polynuclear complex formed by the coordination of Mn^{2+} to two phenoxo oxygens on the Schiff base ligand. We have reported that in the absence of the M^{2+} ion, H_2O_2 decomposition catalyzed by mononuclear [Mn(salen)Cl] proceeds coupled by the Mn(III)–Mn(IV) redox cycle in DMF.[1] The shifts to higher potentials in the presence of the M^{2+} ion easily lead to no oxidation from Mn(III) to Mn(IV) intermediate by H_2O_2 in DMF. This is the reason why the catalytic decomposition is inhibited in the presence of Mn^{2+}, Co^{2+}, Ni^{2+}, and Zn^{2+}. Previously, we reported on the lower uptake for dioxygen by [Co(salen)] in the presence than in the absence of M^{2+}=Mn^{2+}, Co^{2+}, Ni^{2+}, Cu^{2+}, and Zn^{2+} in dimethyl sulfoxide.[19] This result also accounted for the decrease in the electron density at the Co^{2+} ion produced by the coordination of M^{2+} on the Co(II)–M(II) Schiff base complexes.

High Activities of Dinuclear $[Mn(salR)]^+$ (R = en, tnOCOPh)–Cu^{2+} Complexes in DMF. Figure 4A shows the time courses of H_2O_2 decomposition catalyzed by [[Mn-

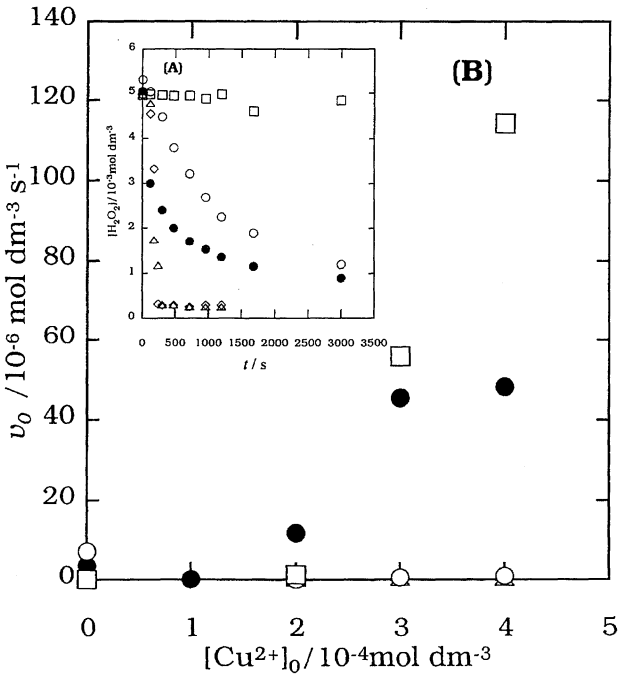

Fig. 4. (A) Time courses of H_2O_2 decomposition catalyzed by $[Mn(salen)]^+$ in the absence and presence of Cu^{2+} in DMF. $[H_2O_2]_0 = 5.00$ mmol dm^{-3}, $[[Mn(salen)]^+]_0 = 0.200$ mmol dm^{-3}, $[Cu^{2+}]_0$ /mmol dm^{-3}: (○); 0, (□); 0.100, (●); 0.200, (△); 0.300, (◇); 0.400 and (B) Plots of v_0 vs. $[Cu^{2+}]_0$. (●); $[Mn(salen)]^+$, (△); $[Mn(saltn)]^+$, (○); $[Mn(saltnOH)]^+$, (□); $[Mn(saltnOCOPh)]^+$.

$(salen)]^+]_0 = 2.00\times10^{-4}$ mol dm^{-3} in the absence and presence of the Cu^{2+} ion. The reaction is effectively inhibited under lower Cu^{2+} concentrations than $[[Mn(salen)]^+]_0 = 2.00\times10^{-4}$ mol dm^{-3} where the trinuclear complex is mainly formed. However, the activities become larger under Cu^{2+} concentrations above 2×10^{-4} mol dm^{-3} where the dinuclear complex may exist mainly in DMF solution. The O_2 evolutions are significantly affected by acrylonitrile as a radical scavenger under $[Cu^{2+}]_0 = 2.25\times10^{-4}$ mol dm^{-3} (Fig. 5), indicating that they include the formation of radical species during H_2O_2 decomposition. As can be seen in Fig. 4B, among $[Mn(saltn)]^+$, $[Mn(saltnOH)]^+$, and $[Mn(saltnOCOPh)]^+$ with the six-membered ring on the 1,3-diamine moiety, the activities of $[Mn(saltn)]^+$ and $[Mn(saltnOH)]^+$ are small even under higher Cu^{2+} concentrations. However, for $[Mn(saltnOCOPh)]^+$ above $[Cu^{2+}]_0 = 3\times10^{-4}$ mol dm^{-3}, the reaction is more accelerated than that for $[Mn(salen)]^+$. Table 5 shows a comparison of the activities under $[Cu^{2+}]_0 = 4.00\times10^{-4}$ mol dm^{-3} for the salen, saltnOCOPh, saltnOH, and saltn complexes. The activities decrease in the following order: saltnOCOPh > salen$\gg$saltnOH > saltn. During H_2O_2 decomposition for $[Mn(salen)]^+$, the spectral changes in the presence of the Cu^{2+} ion are quite different from those in the absence of the Cu^{2+} ion[1] (Fig. 6(A-a)). The final spectrum is in accordance with the spectrum of [Cu(salen)] with the peak at 360 nm, almost substituted by the Cu^{2+} ion. Because in the absence of H_2O_2 the $[Mn(salen)]^+$ is little substituted by the Cu^{2+} ion (Fig. 6(A-b)), it indicates that these spectral changes occur during H_2O_2 decomposition. The formed extent of [Cu(saltnOCOPh)] with the peak at 372 nm (Fig. 6(B-a)) is considerably smaller than that of [Cu(salen)] and is comparable to that in the absence of H_2O_2 (Fig. 6(B-b)). Unfortunately, since the cyclic voltammogram of the Cu^{2+} ion showed a large irreversible redox cycle near to the Mn(II)–Mn(III) redox potential, the cyclic

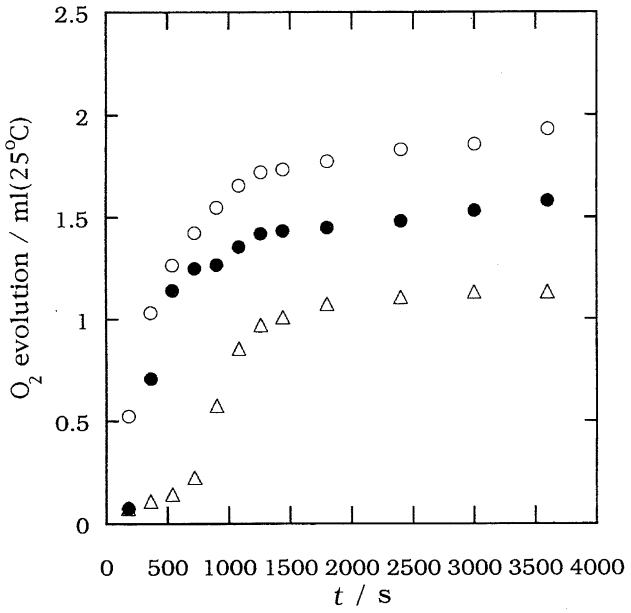

Fig. 5. Time courses of H_2O_2 decomposition catalyzed by $[Mn(salen)]^+$ in the absence and presence of acrylonitrile (AA) in DMF. $[H_2O_2]_0 = 5.00$ mmol dm^{-3}, $[[Mn(salen)]^+]_0 = 0.200$ mmol dm^{-3}, $[Cu^{2+}]_0 = 0.225$ mmol dm^{-3}: $[AA]_0$ /mol dm^{-3}: (○); 0, (●); 0.4 (△); 0.8.

Table 5. Comparison of the Activities of $[Mn(salen)]^+$, $[Mn(saltn)]^+$, $[Mn(saltnOH)]^+$, and $[Mn(saltnOCOPh)]^+$ under $[Cu^{2+}]_0 = 4.00\times10^{-4}$ mol dm^{-3} a)

Ligand	$v_0/10^{-6}$ mol dm^{-3} s^{-1}
saltnOCOPh	114
salen	48.2
saltnOH	0.962
saltn	0.235

a) The values are estimated to be accurate within 10%.

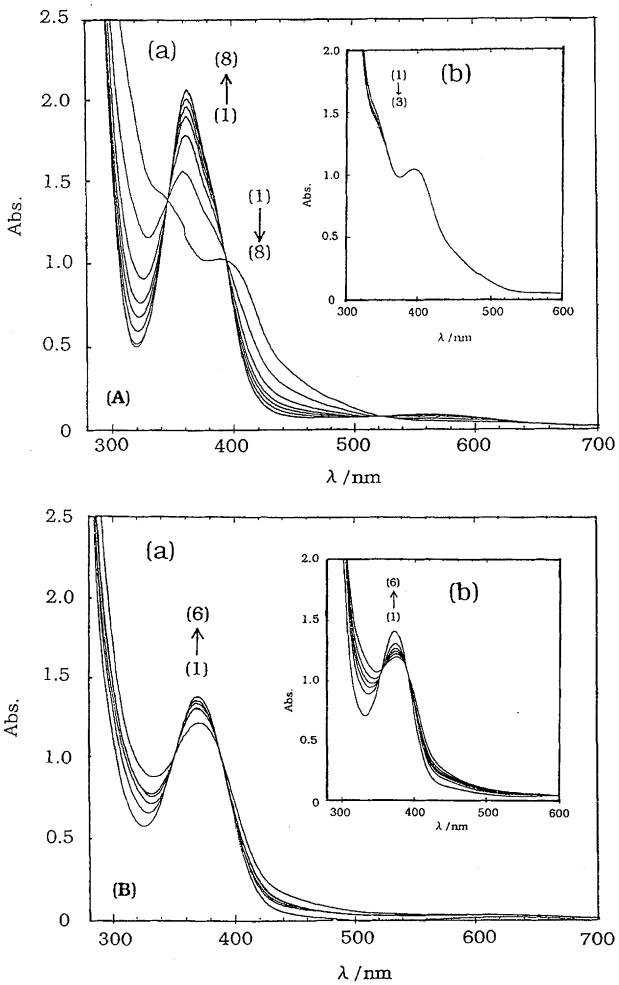

Fig. 6. Spectral changes for $[Mn(salen)]^+$ (A) and $[Mn(saltnOCOPh)]^+$ (B) containing the Cu^{2+} ion in the presence (a) and absence (b) of H_2O_2.
(A): $[[Mn(salen)]^+]_0 = 0.200$ mmol dm^{-3}, $[Cu^{2+}]_0 = 0.200$ mmol dm^{-3}, (a); $[H_2O_2]_0 = 5.00$ mmol dm^{-3}, t /min; (1) 0.5, (2) 5, (3) 15, (4) 20, (5) 30, (6) 60, (7) 90, (8) 210, (b); $[H_2O_2]_0 = 0$ mmol dm^{-3}, t /min; (1) 0.5, (2) 15, (3) 210.
(B): $[[Mn(saltnOCOPh)]^+]_0 = 0.200$ mmol dm^{-3}, $[Cu^{2+}]_0 = 0.300$ mmol dm^{-3}, (a); $[H_2O_2]_0 = 5.00$ mmol dm^{-3}, t /min; (1) 0.5, (2) 5, (3) 10, (4) 20, (5) 30, (6) 60. (b); $[H_2O_2]_0 = 0$ mmol dm^{-3}, t /min; (1) 0.5, (2) 5, (3) 10, (4) 20, (5) 30, (6) ∞.

voltammograms of $[Mn(salen)]^+$ in the presence of the Cu^{2+} ion over the $[Mn(salen)]^+$ concentration were complicated in DMF. Figures 7(a), (b), and (c) show the ESR spectra of the Cu^{2+} ion, the Cu^{2+} ion with $[Mn(salen)]^+$, and after 5 min in H_2O_2 decomposition by $[Mn(salen)]^+$ in the presence of the Cu^{2+} ion at 25 °C, respectively. The ESR spectrum in Fig. 7(a) shows a signal with $g_{\|} = 2.406$ and $g_{\perp} = 2.071$, characteristic of the Cu^{2+} ion in the 250—350 mT range.[20] In the addition of $[Mn(salen)]^+$ to the Cu^{2+} ion solution, a 6-line signal of a small amount of Mn(II) appears in the 300—370 mT range.[20] It strongly suggests that the Mn(II)–Cu(III) complex is partly produced by an intramolecular electron transfer from Cu(II) to Mn(III) on a dinuclear Mn(III)–Cu(II) complex. Further, after 5 min during the H_2O_2 decomposition, the large increase in the Mn(II) signal may depend on metal substitution on a dinuclear Mn(II)–Cu(II) complex, formed by the reaction of a dinuclear Mn(II)–Cu(III) complex with H_2O_2. From the above results, we propose the following catalytic radical mechanism:

$$[Mn^{III}(salR)]^+ + Cu^{2+} \rightleftarrows [Mn^{III}(salR)Cu^{II}]^{3+} \quad (1)$$

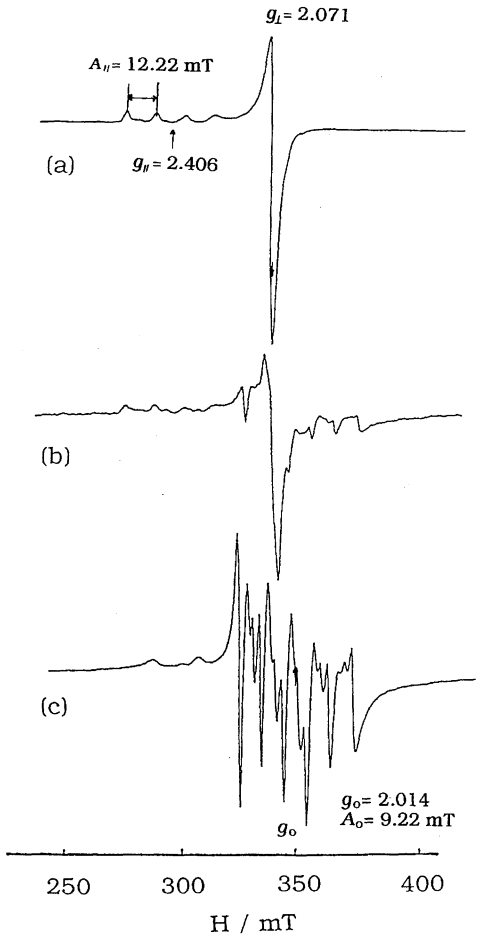

Fig. 7. ESR spectra of Cu^{2+} (a), Cu^{2+} with $[Mn(salen)]^+$ (b), and after 5 min in H_2O_2 decomposition catalyzed by $[Mn(salen)]^+$ in the presence of Cu^{2+} (c). $[Cu^{2+}]_0 = 0.200$ mmol dm^{-3}, $[[Mn(salen)]^+]_0 = 0.200$ mmol dm^{-3}, $[H_2O_2]_0 = 5.00$ mmol dm^{-3}.

$$[Mn^{III}(salR)Cu^{II}]^{3+} \rightleftarrows [Mn^{II}(salR)Cu^{III}]^{3+} \quad (2)$$

$$[Mn^{II}(salR)Cu^{III}]^{3+} + H_2O_2 \rightarrow [Mn^{II}(salR)Cu^{II}]^{2+} + HO_2\cdot + H^+ \quad (3)$$

$$HO_2\cdot + H_2O_2 \rightarrow OH\cdot + O_2 + H_2O \quad (4)$$

$$[Mn^{II}(salR)Cu^{II}]^{2+} + OH\cdot \rightarrow [Mn^{III}(salR)Cu^{II}]^{3+} + OH^- \quad (5)$$

$$[Mn^{II}(salR)Cu^{II}]^{2+} \rightarrow [Cu(salR)] + Mn^{2+} \quad (6)$$
(R = en, tnOCOPh)

Since trinuclear complexes such as [Mn(salR)Cu(salR)-Mn]$^{4+}$ (R = en, tnOCOPh), mainly formed below $[Cu^{2+}]_0 = 2\times10^{-4}$ mol dm^{-3}, are inactive toward H_2O_2, an attack of H_2O_2 to the dinuclear $[Mn^{II}(salR)Cu^{III}]^{3+}$ may occur at not the Mn site, but at the Cu site. The salen donor atoms and salen framework of $[Mn(salen)]^+$ in the crystal are coplanar to each other.[21] The saltnOH framework for $[Mn(saltnOH)(OCOCH_3)]_n$ in the crystal is umbrella-shaped on account of the six-membered ring on the 1,3-diamine moiety.[11] Thus, the saltnOCOPh complex with the 1,3-diamine ligand may have a similar distortion in DMF solution. The coordination of Cu^{2+} to the phenoxo oxygens on the distorted saltnOCOPh complex is more difficult than that on the distorted-free salen complex. In spite of the formation of the unstable dinuclear complex, the acceleration effect is much larger for the saltnOCOPh complex than for the salen complex; furthermore, the substituted extent by Cu^{2+} for $[Mn(saltnOCOPh)]^+$ is smaller than that for $[Mn(salen)]^+$ during H_2O_2 decomposition. The results indicate that for the saltnOCOPh complex the reproduced reaction of $[Mn^{III}(salR)Cu^{II}]^{3+}$, active as catalyst according to Eq. 5, is faster than the metal-substitution reaction according to Eq. 6. As shown in Table 5, among the saltn, saltnOH, and saltnOCOPh complexes with the 1,3-diamine ligand, the saltn and saltnOH complexes show little acceleration effect. The large activity of the saltnOCOPh complex results from the existence of a benzoyloxy group on the 1,3-diamine moiety. It suggests that electron transfer through a benzoyloxy group from $[Mn^{II}(saltnOCOPh)Cu^{II}]^{2+}$ to the OH radical may easily occur to form $[Mn^{III}(saltnOCOPh)Cu^{II}]^{3+}$ and the OH^- ion.

General Conclusions. $[Mn(salen)]^+$ reacts with M^{2+}= Mn^{2+}, Co^{2+}, Ni^{2+}, and Zn^{2+} to give dinuclear Mn(III)–M(II) and trinuclear $Mn(III)_2$–M(II) complexes, resulting in the inhibition of a reaction proceeded by the Mn(III)–Mn(IV) redox cycle. For the Cu^{2+} ion, although the trinuclear complexes are inactive catalysts, the dinuclear complexes (salen, saltnOCOPh) active toward H_2O_2 significantly accelerate the catalytic radical reactions, accompanying metal substitution on the dinuclear complexes in DMF. The high activity of the saltnOCOPh complex in comparison with the salen, saltn, and saltnOH complexes may result from the existence of a benzoyloxy group through which the electron from $[Mn^{II}(saltnOCOPh)Cu^{II}]^{2+}$ to the OH radical easily transfers, producing $[Mn^{III}(saltnOCOPh)Cu^{II}]^{3+}$ as an active catalyst. We have reported that the catalytic reactions of mononuclear

Schiff base Mn(III) complexes in the absence of M^{2+} ion proceed by a two-electron transfer intermolecular reaction coupled by the Mn(III)–Mn(IV) redox cycle.[1)] The activity is the largest for the saltnOH complex on account of stabilization of the transition state for the formation of hydrogen-bondings between the Mn(IV) intermediates and H_2O_2. The formation of polynuclear Schiff base complexes significantly affects the reaction mechanisms and the activities.

The authors acknowledge Prof. Hiromu Sakurai of Kyoto Pharmaceutical University for the measurement of ESR spectra.

References

1) M. Uehara, M. Urade, and Y. Abe, *Bull. Chem. Soc. Jpn.*, **71**, 609 (1998).

2) L. Que, Jr., and A. E. True, *Prog. Inorg. Chem.*, **38**, 97 (1990).

3) J. E. Penner-Hahn, in "Manganese Redox Enzymes," ed by V. L. Pecoraro, Verlag-Chemie, New York (1992), Chap. 2.

4) S. J. Gruber, C. M. Harris, and E. Sinn, *J. Inorg. Nucl. Chem.*, **30**, 1805 (1968).

5) J. M. Epstein, B. N. Figgis, A. H. White, and A. C. Willis, *J. Chem. Soc., Dalton Trans.*, **1974**, 1954.

6) a) "Magnetic Molecular Materials," NATO ASI Series E, ed by D. Gatteschi, O Kahn, J. Miller, and F. Palascio, Kluwer Academic, Dordrecht, Holland (1991), Vol. 198; b) O. Kahn, "Molecular Magnetism," VCH Verlagsgesellshaft, Weinheim, Germany (1993).

7) a) Y. Naruta, M. Sasayama, and K. Maruyama, *Chem. Lett.*, **1992**, 1267; b) A. Gelasco and V. L. Pecoraro, *J. Am. Chem. Soc.*, **115**, 7928 (1993); c) P. J. Pessiki and G. C. Dismukes, *J. Am. Chem. Soc.*, **116**, 898 (1994); d) H. Wada, K. Motoda, M. Ohba, H. Sakiyama, N. Matsumoto, and H. Okawa, *Bull. Chem. Soc. Jpn.*, **68**, 1105 (1995); e) M. Delroisse, A. Rabion, F. Chardac, D. Tetard, J. Verlhac, L. Fraisse, and J. Seris, *J. Chem. Soc., Chem. Commun.*, **1995**, 949.

8) G. C. Dismukes, "The Organization and Function of Manganese in the Water-Oxidizing Complex of Photosynthesis," Academic Press, New York (1986), Chap. 16.

9) P. Pfeiffer, E. Breith, E. Lubbe, and T. Tsumaki, *Ann.*, **503**, 84 (1933).

10) N. Kitajima, K. Whang, Y. Moro-oka, A. Uchida, and Y. Sasada, *J. Chem. Soc., Chem. Commun.*, **1986**, 1504.

11) J. A. Bonadies, M. L. Kirk, M. S. Lah, D. P. Kessissoglou, W. E. Hartfield, and V. L. Pecoraro, *Inorg. Chem.*, **28**, 2037 (1989).

12) J. T. Donoghue and R. S. Drago, *Inorg. Chem.*, **1**, 866 (1962).

13) Y. Abe, K. Morikawa, and M. Kikukawa, *Polyhedron*, **7**, 2135 (1988).

14) "SIR92," A. Altomare, M. C. Burla, M. Camalli, M. Cascarano, C. Giacovazzo, A. Guagliardi, and G. Polidori, *J. Appl. Crystallogr.*, **27**, 435 (1994).

15) "DIRDIF94," P. T. Beurskens, G. Admiraal, G. Beurskens, W. P. Bosman, R. de Gelder, R. Israel, and M. M. Smits, The DIRDIF94 Program, Technical Report of the Crystallography Laboratory, University of Nijmegen, The Netherlands (1994).

16) D. Hall and T. N. Waters, *J. Chem. Soc.*, **1960**, 2644.

17) T. P. Cheeseman, D. Hall, and T. N. Waters, *J. Chem. Soc. A*, **1966**, 1396.

18) N. Galesic and R. Trojko, *Acta Crystallogr., Sect. C*, **C40**, 232 (1986).

19) Y. Abe, K. Shinguhara, and Y. Yano, *Chem. Lett.*, **1992**, 897.

20) H. Sakurai, "Practice of Electron Spin Resonance Spectrum," Hirokawa Publishing Co., Tokyo (1992).

21) V. L. Pecoraro and W. M. Butler, *Acta. Crystallogr., Sect. C*, **C42**, 1151 (1986).